Tiling of a Nb(110) surface with NbO crystals nanosized by the NbO/Nb misfit

I. Arfaoui,[1,2,*] J. Cousty,[1,†] and H. Safa[2]
[1]*Commissariat à l'Énergie Atomique, Service de Physique et Chimie des Surfaces et Interfaces, Centre d'Études de Saclay, F-91191 Gif sur Yvette, France*
[2]*Commissariat à l'Énergie Atomique, Service d'Études des Accélérateurs, Centre d'Études de Saclay, F-91191 Gif sur Yvette, France*
(Received 2 July 2001; published 7 March 2002)

The overlayer covering a (110) face of a Nb crystal annealed at 1500–2000 K in UHV has been studied by Auger electron and photoemission spectroscopies, low-energy electron diffraction (LEED) and scanning tunneling microscopy (STM). This layer, which results from the surface segregation of oxygen dissolved in Nb bulk, corresponds to a thin niobium oxide with a $NbO_{x\approx 1}$ stoichiometry as shown by photoemission with synchrotron radiation. Both LEED and STM investigations show the complex structure of the oxide overlayer with two orientations rotated by 109°. LEED diagrams reveal the epitaxial relationship between lattices of the oxide overlayer and the metal. From STM observations, each domain in the oxide layer consists of a quasiperiodic arrangement of strictly parallel sticks. Analysis of all the results shows that each stick characterizes a small NbO crystal with a typical $3.5\times 1.4\ nm^2$ size. Therefore, the oxide layer can be described as a side to side arrangement of these NbO nanocrystals (fcc) on Nb(110) (bcc). Two kinds of epitaxial relationship between these two lattices are found: (i) the relative arrangement of NbO nanocrystals is determined by the underlying Nb(110) lattice; (ii) each nanocrystal develops an epitaxy relationship with the metal surface since the NbO lattice presents one (111) plane parallel to Nb(110) and one NbO ⟨110⟩ direction is parallel to one Nb ⟨111⟩ direction (Kurdjumov-Sachs-type alignment). The origin of this structure is discussed in terms of NbO/Nb misfit.

DOI: 10.1103/PhysRevB.65.115413 PACS number(s): 81.10.−h, 81.65.Mq, 68.55.Ac

I. INTRODUCTION

Many technological applications of metals are determined by the properties of the thin oxide layer, which covers them. In the particular case of niobium, which is often used as a superconducting material, the presence of oxides influences the concentration of oxygen atoms in the bulk and then the superconducting properties of the underlying metal. For high technology applications of this metal in nanoelectronic devices[1] (Josephson junctions) and superconducting high-frequency cells for accelerating particles,[2] the oxide crystal structure and its epitaxial relationship with the metal substrate are then issues of fundamental interest. For example, the maximum value of the electric field supported by the internal surface of an accelerating cell is limited by properties of the Nb surface but also by those of the oxide overlayer.[2] Specifically, the thin conductive layer near the surface plays a critical role for these cells because high frequencies are used. As these cells are usually made with thick niobium plates, many studies have been devoted to properties of niobium and niobium oxides.[3–24] In particular, Hallbritter proposed that a Nb surface exposed to air is covered by a sequence of several Nb oxides with different stoichiometries: Nb_2O_5, NbO_2 and NbO (Refs. 13–15). It is also known that a three-dimensional (3D) NbO oxide presents metallic properties while the 3D oxygen-rich oxides, as NbO_2 and Nb_2O_5, are semiconductor and insulating materials, respectively. So a niobium surface covered by an oxide layer appears as a very complex system with several interfaces. In an attempt to simplify the investigated system, several studies have been focused on the NbO/Nb interface. Investigations by Auger electron spectroscopy (AES) and/or x-ray photoemission spectroscopy (XPS) of a Nb sample heated in UHV have shown that a thin layer of NbO covers the metal surface.[16,17] Such an oxide overlayer was attributed to the surface segregation of the oxygen atoms dissolved in the Nb crystal after annealing. The structure of this oxide layer mainly studied by (low-energy electron diffraction) LEED was assigned to a crystallized NbO overlayer (fcc-like crystal). In fact, the NbO crystal was proposed to be in partial epitaxy on the metal lattice with a (111) face parallel to the Nb surface and one NbO ⟨110⟩ direction parallel to a Nb ⟨111⟩ close packed direction.[7,8] Very recently, a scanning tunneling microscopy (STM) and RHEED (reflection high-energy electron-diffraction) study devoted to the oxygen-induced surface structure of Nb(110) has been reported.[20] The STM images show a quasiperiodic arrangement of small protrusions with some defects. From these images and RHEED measurements, the authors have proposed a description of the NbO layer in opposition with the previously reported results.[7,8,18]

In this paper, we present a study of the thin niobium oxide overlayer grown on a (110) surface of a single Nb crystal after annealing in UHV by combining AES, photoemission spectroscopy with synchrotron radiation, LEED, and STM. In particular, STM images reveal the quasiperiodic structure of linear features in the oxide layer covering (110) Nb. Analysis of all these data allows us to propose a structural model of this $NbO_{x\approx 1}$ overlayer that develops some preferential orientations in relation with the surface lattice of the underlying metal.

II. EXPERIMENT

The experiments were performed in three separate UHV chambers, which were fitted with an ion gun and an electron

gun for heating the sample. One chamber with a base pressure of 2×10^{-11}–4×10^{-11} mbar is equipped with a STM (Omicron1), a cylindrical mirror analyzer for *in situ* AES (Omicron 100), and facilities for transferring samples and STM tips. The LEED experiments (Omicron) were performed in the second chamber with a base pressure of 2×10^{-11}–4×10^{-11} mbar. Spectroscopy measurements on Nb 3*d* core levels were made with synchrotron radiation at LURF (Orsay, France) on the line (SA 73) in the third chamber with a base pressure of 1×10^{-10}–3×10^{-10} mbar also equipped with a LEED system. The overall resolution of the experimental setup (photon monochromator and electron analyzer) is 200 ± 20 meV.

STM tips were electrochemically etched from a W wire (diameter$=0.25$ mm) in a KOH solution ($1M$). In vacuum, these tips are cleaned by ion sputtering and sometimes suffer *in situ* -10 V pulses during scanning particularly to achieve high-resolution images. All the STM images were recorded at room temperature in the constant current mode (topography mode) and were only submitted to subtraction of the background plane.

Three samples (discs 6 mm in diameter and 2 mm thick) which were cut in a single crystal of Nb (Goodfellow) were mechanically polished and chemically etched. The surface orientation was checked by x-ray back diffraction [$\pm3°$ from (110) plane for two samples and $\pm0.5°$ for the other]. Estimation of the crystal purity by resistivity measurements gives an overall concentration of impurities of $\sim$500 ppm (mainly oxygen).[21] After etching in a mixture of acids (HF:1, HNO_3:1, H_2PO_4:2), the crystals were rinsed with deionized water and dried under a flux of pure nitrogen before to be mounted on the sample holder. In vacuum, the surfaces were further cleaned by many cycles of Ar^+ sputtering (1 keV) and annealing at temperature in the 1200–2200 K range (typical duration 20–30 min). No significant changes in the structure and the chemical composition of the surface were detected for a sample annealed at 1200 K or at 2200 K.

III. RESULTS

We quickly present the AES and photoemission results then report the LEED and STM investigations on the overlayer covering the Nb(110).

After sputtering, AES spectra of the surface show mainly the presence of Nb peaks with very small ones attributed to carbon and nitrogen. After annealing and cooling down to 300 K, an extra peak appears at 510 eV attributed to oxygen. Taking in account the base pressure in the chamber, the origin of this oxygen is attributed to surface segregation of O atoms diluted in the Nb bulk during the annealing process in agreement with previous studies. The measured ratio of O and Nb peak heights is equal to 0.2 ± 0.02. Such a value agrees well with previous measurements.[12] According to this work, the overlayer is identified with a thin NbO film covering the Nb metal. The presence of this oxide layer is confirmed by the first photoemission spectroscopy measurements performed on this system with synchrotron radiation. With 260-eV photons, the mean-free-path length for Nb 3*d* is very low (typically 0.5 nm) and the contribution of Nb atoms within the thin oxide layer to the 3*d* Nb photoemission spectra becomes maximum as shown in Fig. 1. This spectrum presents four well-resolved peaks A, B, C, and D that are assigned to two couples of $3d^{5/2}$ and $3d^{3/2}$ Nb core levels. One couple of peaks (A and C) originates from Nb atoms in a metal state.[9] Taking in account the 1.4-eV energy shift towards higher binding energies when compared to the metal peaks, the other couple (B and D) is attributed to Nb atoms in the oxide layer.

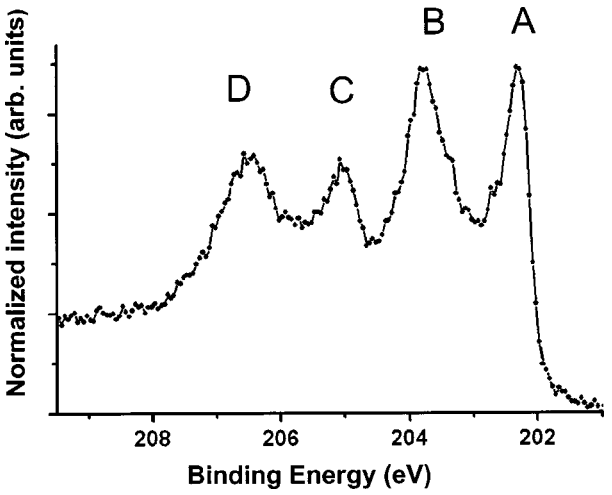

FIG. 1. Photoemission spectra of the 3*d* Nb core levels from an annealed Nb (110) surface with 260 eV photons (synchrotron radiation). Peaks *A* and *C* at 202.2 ± 0.1 eV and 205.1 ± 0.1 eV correspond to $3d^{5/2}$ and $3d^{3/2}$ levels of Nb atoms in metal. Peaks *B* and *D* at 203.7 ± 0.1 eV and 206.5 ± 0.1 eV are shifted by 1.4 eV from *A* and *C*, respectively. Peaks *B* and *D* are associated to Nb 3*d* levels in the $NbO_{x\approx1}$ overlayer.

In general, a complex LEED pattern with two orientations of a superstructure is observed in agreement with previous studies.[7,8] However, some parts of the surface of the well-oriented crystal display a single orientation as shown in Figs. 2(a) and 2(b). These figures reveal also the presence of some large spots for the oxide layer and an absence of spots in several parts of the diagram. We point out that the thin oxide overlayer exhibits a strongly anisotropic structure since the superstructure spots are arranged in streaks [Fig. 2(b)]. From analysis of these LEED patterns taken with electron energy ranging from 52 to 200 eV, we deduce that:

(i) The oxide lattice shows a slightly distorted sixfold symmetry since the vectors **b**1 and **b**2 have different lengths ($|\mathbf{b}1|/|\mathbf{b}2|=1.02$). The angle values in this pseudohexagonal cell vary from 58 ± 1 to $62\pm1°$ [Fig. 2(a)]. Taking into account these data together with the spots issued from the Nb crystal, this diagram corresponds to a distorted NbO lattice with one (111) plane parallel to the Nb(110) surface.

(ii) One $\langle110\rangle$ direction of the NbO(111) plane is parallel to one $\langle111\rangle$ direction of the Nb(110) surface [Fig. 2(a)].

(iii) The superstructure of the oxide presents a four-period along one $\langle111\rangle$ of the Nb lattice [Fig. 2(b)]. Although, the superstructure lattice is not well defined in many parts of the LEED diagram, a typical elementary cell can be defined. The

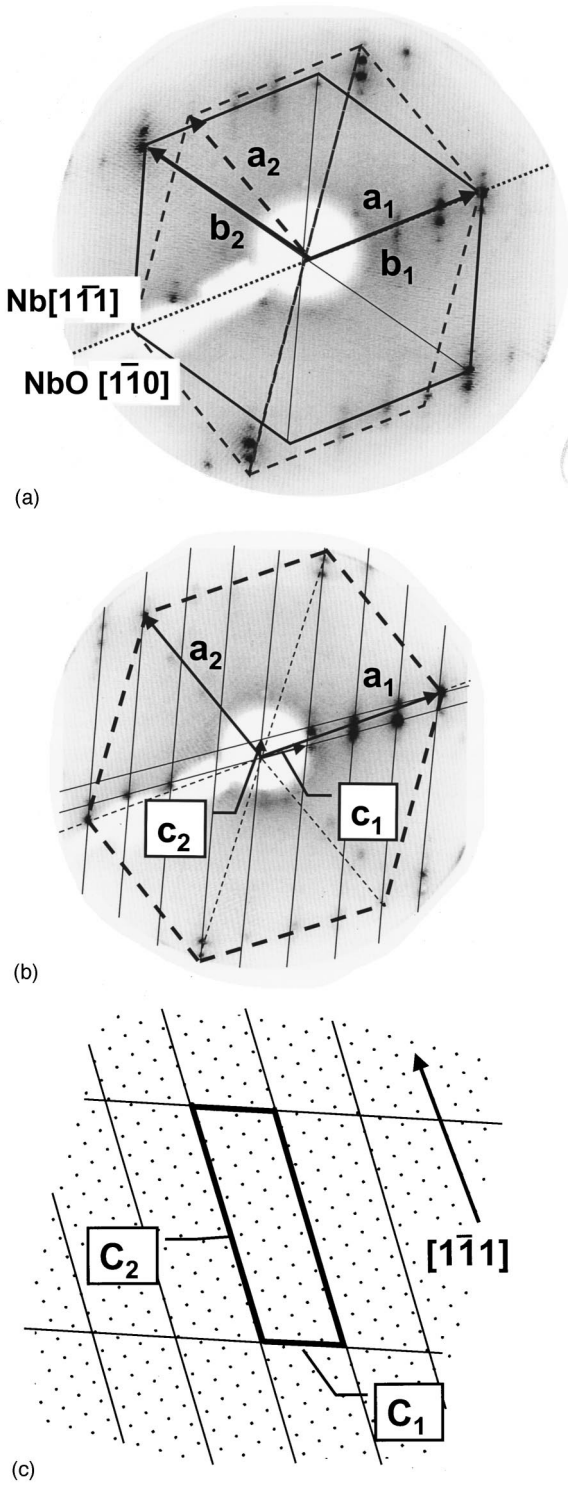

FIG. 2. LEED diagrams of an annealed (110) Nb surface showing a single orientation of overlayer domains. (a) The cells of Nb (110) and Nb oxide are indicated by dashed lines and continuous lines, respectively. The hexagon of the oxide lattice is slightly distorted ($E=75$ eV). (b) The superstructure of the oxide layer defined by vectors **c**1 and **c**2 corresponds to a pseudocoincidence cell with respect to Nb (110) lattice. The thin lines indicate the streak orientation ($E=52$ eV). (c) Real space cell of the superstructure shown in (b). The typical size of this cell is 3.5×1.4 nm^2. Black dots are for Nb atoms.

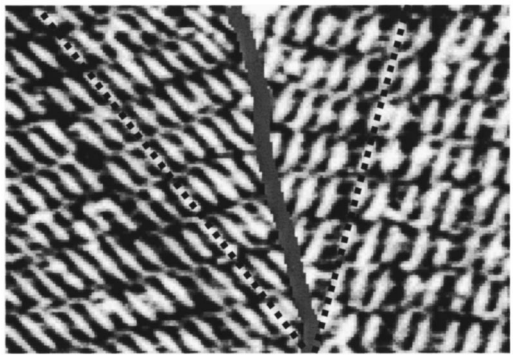

FIG. 3. Typical large scale STM image showing two domains characterized by one direction of white stripes (dotted lines) made of small sticks. The density of these stripes changes along a domain as shown in the right part of the image. The angle between sticks in the two domains is equal to $70°\pm2°$. ($Vb=-1$ V, $It=17$ nA 22×30 nm^2).

corresponding cell ($C1$, $C2$ in the real space) is determined by the following relations:

$$C_1=4.2\,\mathbf{A}_1-3.1\,\mathbf{A}_2,$$

$$C_2=1.4\,\mathbf{A}_1+11.8\,\mathbf{A}_2,$$

with $\mathbf{A}_1$ and $\mathbf{A}_2$ the vectors of the Nb(110) lattice. This cell with a parallelogram shape (3.5×1.4 nm^2 area) corresponds to a pseudocoincidence lattice between the overlayer and the Nb surface [Fig. 2(c)].

Large-scaled STM images on samples with a low density of steps show that the oxide layer covering the Nb(110) face consists of white stripes roughly parallel along two main directions, which determines two types of domains within the overlayer (Fig. 3). The local density of these stripes exhibits fluctuations along the surface. At higher resolution, the stripes appear as the result of a particular arrangement of short and prominent sticks. In fact, the oxide overlayer is formed by a quasiperiodic arrangement of these sticks, which

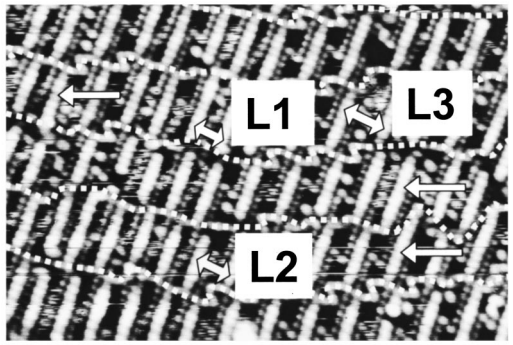

FIG. 4. Typical STM image showing the quasiperiodic arrangement of parallel sticks generating a lamella structure (single arrows show sticks and the dotted lines follow the boundaries between the lamella). The distance between neighboring sticks along a lamella is quantized since only three values are measured: $L1$, $L2$, and $L3$ (double arrows) ($Vb=1$ V, $It=17$ nA 13×20 nm^2).

TABLE I. Ratios of distances $Li/L1$ measured between neighboring sticks along lamella and of distances $Di/D1$ measured between neighboring sticks in neighboring lamella ($L1$ and $D1$ the shortest distances).

	$L2/L1$	$L3/L1$	$D2/D1$	$D3/D1$
Expt value	1.25 ± 0.03	1.5 ± 0.03	2 ± 0.1	3 ± 0.1

stay remarkably parallel (Fig. 4). Several measurements reveal that the angle between sticks in different domains is equal to $109\pm2°$ that corresponds well to the angle (109.2°) between ⟨111⟩ closed packed directions of (110) Nb. We also remark that the stick length shows a very small dispersion since hundreds of measurements give $L=3\pm0.3$ nm for large terraces. As a result, the packing of these parallel sticks can be described as a lamellalike arrangement (Fig. 4). However, we have frequently observed defects in both the stick packing (stacking faults) and in the sticks. Careful analysis of STM images reveals that the stick arrangement exhibits unique properties: (i) Along a lamella direction, there exist only a few values for the distance between neighboring sticks. From hundred measurements on more than 10 different areas on two samples, we have found three values for the distances between neighboring sticks $L1$, $L2$, and $L3$ (Fig. 4). As distance ratios eliminate the influence of piezoelectric drifts in STM measurements, the different ratios reported in Table I clearly demonstrate that the distances between neighboring sticks are quantized. The histogram of $L1$, $L2$, and $L3$ distances measured on several images obtained on large terraces (not shown) reveals that the most frequent distances are $L1$, then $L2$, and a few $L3$. (ii) Parallel to the stick direction, neighboring sticks in neighboring lamella are shifted by distances, which are also quantized. As illustrated in Fig. 5, we

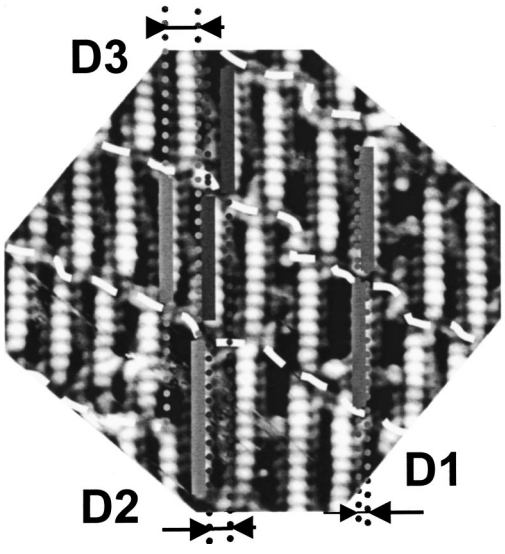

FIG. 5. Lateral shifts between sticks in neighboring lamella are also quantized since only three distinct values are measured in several STM images ($D1$, $D2$, and $D3$). In a very few cases (5 on about 250 measurements), we have found two aligned sticks. The alignment of bumps forming each stick is clearly observed.

TABLE II. Ratio of distances Li and Di on the shortest distance between neighboring sticks $D1$. The values demonstrate the existence of an epitaxial relationship of the NbO overlayer and the Nb (110) lattice. $D1$ was measured on the same image than Li or Di in order to compensate the piezo drift.

	$D2/D1$	$D3/D1$	$L1/D1$	$L2/D1$	$L3/D1$
Expt value	2 ± 0.1	3 ± 0.1	4 ± 0.1	5 ± 0.1	6 ± 0.1

also measured three distinct values for these distances, $D1$, $D2$, and $D3$. As $D1$ is the smallest distance for this lateral shift, we report ratios of these distances in Table II. Remarkably, these ratios present integer values.

The high-resolution image shown in Fig. 5 demonstrates that the prominent sticks are formed by a close-packed alignment of typically 10 ± 1 bumps separated by 0.3 ± 0.05 nm (Figs. 4 and 5). Therefore, the sticks appear as a part of a dense direction of the NbO crystals. Finally, many STM images (Figs. 3–5) reveal some poorly ordered area in between sticks. In particular, Fig. 4 shows the presence of prominent lines in between the lamellas, which exhibit some regular meanders. In between straight and prominent sticks, there exist *S*-shaped alignments of dark bumps.

IV. DISCUSSION

From all of these results, we propose a nanometer-scaled model of the oxide overlayer based on the self-arrangement of small niobium oxide crystals. This section organizes in three parts devoted to (i) the model of the niobium oxide nanocrystals, (ii) the packing of these nanocrystals, and (iii) a discussion of this model focusing on the role of the misfit between the two involved lattices.

A. A nanometer-scaled model of small niobium oxide crystals

We first consider the oxide stoichiometry. From core-level shifts on 3D niobium oxide,[9,22] the expected shift between $3d$ levels of Nb atoms in metal and in NbO is 1.8 ± 0.1 eV. So, the 1.4 eV shift measured on the oxide overlayer indicates that no stoichiometric NbO compounds cover the niobium surface. Furthermore, peaks B and D related to Nb atoms in the oxide appears much larger than those obtained by Strisland *et al.* with similar experimental conditions on a clean Nb (110).[25] This suggests that the oxide layer presents several stoichiometries close to NbO. Details about these NbO compounds will be given elsewhere.[25,26] For the oxide thickness, only estimation can be deduced from this spectrum. Taking into account a very short attenuation length for 50–55 eV photoelectrons,[27] we estimate that the oxide contains 1 to 2 layers of Nb atoms.

To elucidate the complex structure of this overlayer would require direct information on the relationship between the NbO layer and the metal lattice. In absence of STM images of the metal surface since the oxide layer covers the entire Nb (110) face, we compare LEED data to STM observations in order to get deeper insights on the NbO/Nb (110) system.

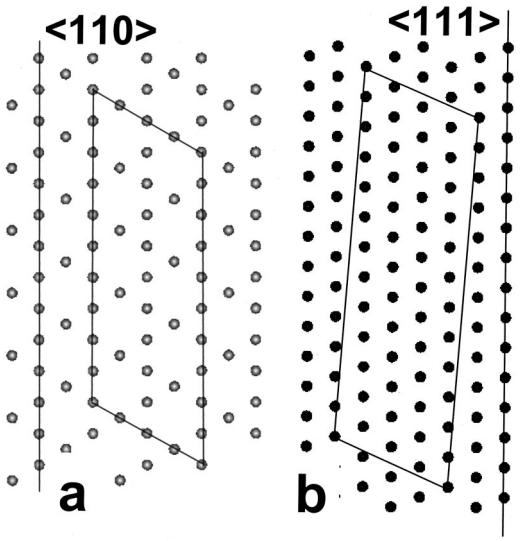

FIG. 6. (a) Atomic model of a (111) Nb plane of a NbO crystal. The cell represents a top view of a template for one NbO nanocrystal. (See text for details.) (b) Cell of the superstructure deduced from the arrangement of NbO nanocrystals on the Nb (110) lattice shown in Fig. 8.

LEED patterns have shown that the (111) plane of distorted NbO crystals is parallel to the (110) Nb surface with one NbO ⟨110⟩ direction parallel to one Nb ⟨111⟩ direction. A qualitative analysis of these patterns also indicates that the presence of small crystals together with stacking faults in their packing.[28]

As the parallel sticks observed in STM images are formed by a close-packed arrangement of bumps with a 0.3 nm spacing, they can be assigned to segments of close-packed ⟨110⟩ NbO rows since the smallest atomic period along ⟨110⟩ NbO is equal to 0.298 nm. Since NbO ⟨110⟩ is parallel to Nb ⟨111⟩, this identification is consistent with the 109° angle measured between sticks in two domains. Let us now consider the different ratios of $D2$, $D3$, $L1$, $L2$, and $L3$ on the shortest measured distance $D1$ (Table II). Interestingly, these ratios have only integer values within the accuracy of measurements. These integer values then demonstrate that the relative positions of sticks are connected to a lattice. As the angle measured between sticks in two domains is 109° [instead of 120° for ⟨110⟩ on a large NbO (111) lattice], we deduce that the organization of these segments of NbO ⟨110⟩ directions is determined by the underlying Nb (110) surface.

Considering both the stick arrangement and the existence of NbO crystals with a (111) plane parallel to the metal surface, we propose that each stick is associated with a small NbO crystal. Obviously, the length and width of these NbO crystals are related to the stick length and to the distance in between neighboring sticks in a lamella, respectively. Taking into account the quantization of the distance between sticks, a template of a nanocrystal could present the shape shown in Fig. 6(a). Since each NbO crystal presents a surface parallel to (111) plane, it is reasonable that the edges are parallel to NbO ⟨110⟩ directions making a 60° (120°) angle. As a result, the longest edges of the nanocrystal are parallel to Nb ⟨111⟩. The nanocrystal width is equal to the distance separating four

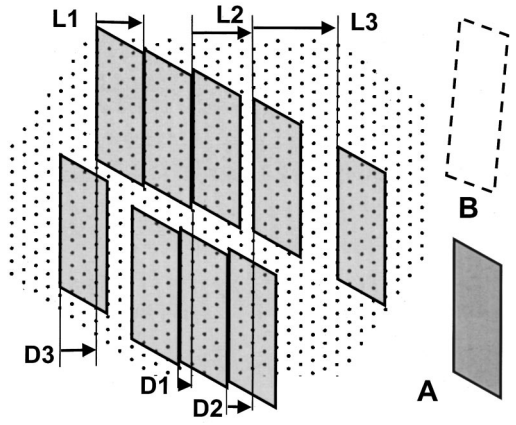

FIG. 7. Model of packing of self-assembled NbO nanocrystals, which are tiling the Nb (110) surface. Depending on the relative arrangement of nanocrystals on the Nb (110) surface, one reproduces the typical distances measured on STM images (*Li* and *Di*). This model illustrates the epitaxial relationships between the NbO nanocrystals and Nb (110) surface. However, this rigid model cannot account for the poorly ordered boundaries between lamella. Gray parallelograms are for NbO nanocrystals (*A*). Parallelogram with dashed lines is for a cell of the periodic packing of nanocrystals (*B*). The black dots are for Nb atoms.

⟨110⟩ rows of NbO since the coincidence period observed in LEED diagram is about four, which agrees well with the smallest distance measured in between sticks ($L1$). The origin of the stick relief observed in STM images will be discussed elsewhere.[25]

B. Organization of NbO nanocrystal

In this framework, the oxide overlayer consists in a side-to-side packing of the NbO nanocrystals. We stress that the self-organization of these nanocrystals depends on the lattice of the underlying (110) Nb surface as illustrated in Fig. 7. This schematic diagram provides a typical example of how to tile a Nb (110) surface with nanometer-scaled NbO crystals. In particular, the examples of stacking faults in the nanocrystal packing shown in this figure correspond to translation of neighboring nanocrystals by different vectors of the Nb (110) lattice. Thereby, for a stick attached to each nanocrystal, this model reproduces the main features observed with STM such as, for example, the quantization of the Li and Di distances and the lamella structure. Such a substrate-induced quantization of stacking fault amplitudes in the adsorbate packing has been reported in several heteroepitaxial systems.[30]

For some areas of the NbO Nb system in which a quasi-periodic arrangement of nanocrystals has grown (Fig. 8), one can describe, in this framework, the corresponding cell in terms of Nb (110) lattice.

$$C_1 = 4\,\mathbf{A}_1 - 3\,\mathbf{A}_2,$$

$$C_2 = 1\,\mathbf{A}_1 + 12\,\mathbf{A}_2.$$

Such a cell defines a coincidence lattice very close to the one presented in Fig. 6(b). Furthermore, this cell appears similar

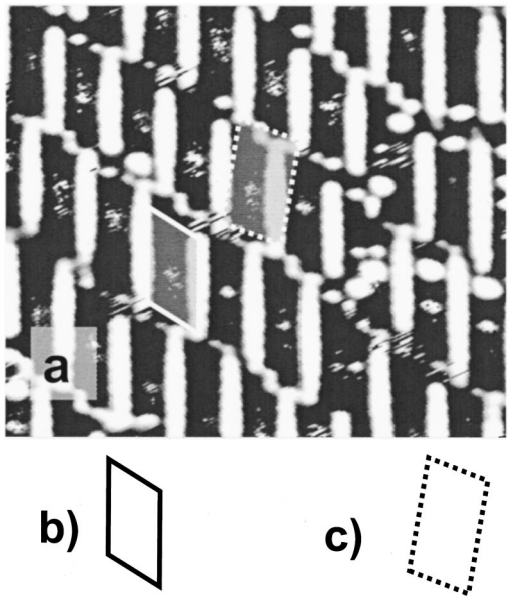

FIG. 8. STM image of a selected area with a quasiperiodic arrangement of sticks (a). Parallelograms indicate an envelope of a nanocrystal containing a stick (b) and an elementary cell of this quasiperiodic arrangement (c).

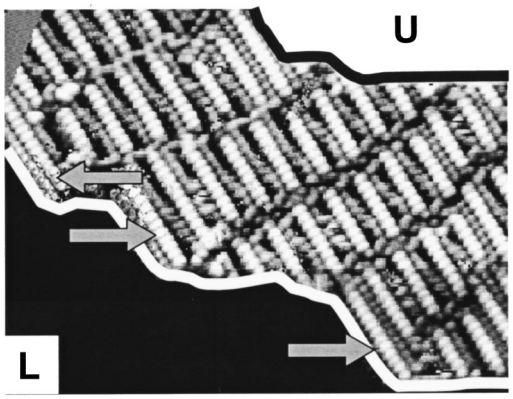

FIG. 9. STM image of one terrace of a stepped NbO/Nb surface. Continuous black and white lines indicate step edges. Upper and lower terraces noted *U* and *L* are white and black, respectively, in order to obtain a good contrast in the middle terrace. The long sticks with 13 bumps (gray arrows) are mainly present near the step edge. We point out that sticks are parallel to parts of the step edge.

to the one deduced from LEED diagrams (Fig. 2c). In fact, the cell shown in Fig. 2(c) characterizes an average cell since the electron beam probes several μm^2 of the surface. The presence of fluctuations in the nanocrystal sizes observed in STM images is consistent with our LEED diagrams.

Finally, there exist two levels in the epitaxial relationships of NbO nanocrystals on Nb (110). The first one is related to the relative arrangement of NbO nanocrystals in the overlayer and the Nb (110) surface. The second level of epitaxy concerns the orientation of the lattice of each nanocrystal on Nb (110). A NbO (111) face parallel to Nb (110) together with one ⟨110⟩ direction of each NbO crystal parallel to Nb ⟨111⟩ corresponds to a Kurdjumov-Sachs (KS) epitaxial relationship. This is consistent with theoretical models proposed for a thin layer with a (111) fcc lattice on top of a (110) bcc crystal with a misfit $(d_{fcc}-d_{bcc})/d_{bcc}=0.04$.[29] Such a value does correspond to the misfit value of NbO (111)/Nb (110) along their common direction (NbO ⟨110⟩ 0.2977 nm and Nb ⟨111⟩ 0.2858 nm).

C. Discussion of the model

Although the NbO/Nb misfit is small (+4%), some evidences of distortions in the lattice of the thin NbO nanocrystals can be found in both STM images and LEED patterns. For example, we remark that the stick length presents a larger dispersion in many STM images of stepped surfaces than on those obtained on large terraces. Analysis of stick lengths reveals that the sticks located near a step edge and parallel to the edge are generally longer than those located in the middle of large terraces as illustrated in Fig. 9. As relaxation of the strain induced by NbO/Nb misfit could be easier near a step edge, we infer that the presence of longer sticks observed only in the vicinity of step edges reveals the influence of the misfit on the nanocrystal size. In consequence, we deduce that the NbO/Nb misfit limits the extension of NbO crystals at 2.7–3 nm along ⟨110⟩ NbO on large Nb (110) terraces. We notice also that sticks are strictly parallel to some step edges, which supports the above-proposed orientation of the stick on Nb (110). On the other hand, we have remarked that LEED patterns of the (111) NbO overlayer suffer some distortions, which provide another evidence of this strain.

In any case, this nanometer-scaled model based on self-assembled nanocrystals with numerous packing defects provides a good description of the main results obtained on NbO/Nb (110). Such a model appears very different from the one proposed by Pantel, Bujor, and Bardolle.[8] In particular, the disordered interlamella boundaries and the presence of both nanosized NbO crystals and stacking faults in between these crystals was completely ignored. Furthermore, the periodicity in their LEED diagrams does not correspond to the cell we observed. Very recently, a STM study of the reconstruction of a Nb (110) surface induced by the segregation of oxygen has been reported.[20] While these images show some similarities with our STM observations, we never observe triangular-shaped features in our images. A different epitaxial relationship between the oxide layer and Nb (110) than the one presented above have been proposed since the ⟨110⟩ NbO is turned off by 5° from the ⟨111⟩ close-packed direction of Nb (110). A possible origin of these different arrangements could be related to differences in the stoichiometry and/or thickness of the oxide overlayer induced by differences in the bulk oxygen concentration and/or in cooling speed, which determines the amount of segregated oxygen at the sample surface. For instance for Pd overlayers on chromium surfaces, either a KS or Nishiyama-Wasser epitaxial relationship was found depending on the Pd thickness.[31]

However, we notice that sticks in their STM images of NbO/Nb system are parallel to step edges in agreement with our observations and with data reported by Flynn *et al.*[18] On the other hand, Robach *et al.* have concluded that the epitaxial relationship between a thin TaO crystal and a Ta (110) surface corresponds to a Kurdjumov-Sachs orientation.[32] Monoxide NbO and TaO crystals develop then the same epitaxial relationship with a (110) surface of the corresponding metal, which belong to the same column of periodic table. A similar model based on SnO nanocrystals tiling a Pt (111) surface has been proposed for describing the complex structure of this system.[33] Finally, the structure on a Nb (100) surface annealed at 1300 K in UHV studied by STM is explained by the formation of big nanocrystals[34] (30 nm length).

V. CONCLUSION

In this paper, we have studied, by combining AES, photoemission spectroscopy, LEED, and STM methods, the oxide overlayer covering a Nb (110) surface after annealing in UHV. The oxide layer that results from the surface segregation of the oxygen dissolved in the Nb bulk presents a stoichiometry close to NbO as shown by photoemission spectroscopy with synchrotron radiation at LURE. The complex structure of this oxide overlayer can be described as a quasiperiodic self-organization of lamella separated by narrow meandering stripes. Each lamella results from a side-to-side arrangement of NbO nanocrystals, which is governed by the underlying Nb (110) lattice. For each NbO crystal, the (111) plane is parallel to the Nb (110) surface and one ⟨110⟩ direction is parallel to one Nb ⟨111⟩. The orientation of the two lattices corresponds to a Kurdjumov-Sachs epitaxial relationship. Such a tiling of the Nb (110) surface by a self-assembled arrangement of rigid $NbO_{x\approx 1}$ nanocrystals is then the first structural model of a NbO/Nb (110) crystal prepared in UHV. However, this self-organization presents a high density of defects. Several evidences of distortions in the lattice of $NbO_{x\approx 1}$ nanocrystals induced by the misfit with the underlying Nb (110) surface are also found. In particular, the length of NbO nanocrystals appears to be related to the misfit along Nb ⟨111⟩. By construction, the proposed rigid model cannot account for these distortions and for the disordered parts in between lamella observed in STM images. Finally, studies devoted to the influence of stoichiometry variations in the oxide overlayer on its structure would provide deeper insights on this important interface for some high technology applications.

ACKNOWLEDGMENTS

We would like to thank C. Guillot, C. Antoine, B. Delomez, and N. Barrett for their help in photoemission measurements at LURE and C. Lubin, F. Merlet, P. Lavie, F. Thoyer, and A. Vittiglio for technical support.

*Permanent address: EPFL, DP IPE, CH 1015 Lausanne, Switzerland.

†Corresponding author. Email address: cousty@cea.fr

[1] I. Kagan, A. J. Leggett, V. M. Agranovich, and A. A. Maradudin, in *Quantum Tunnelling in Condensed Media (Modern Problems in Condensed Matter Sciences)*, edited by Yu. Kagan and A. J. Leggett (North-Holland, Amsterdam, 1992).

[2] H. Padamsee, K. Knobloch, and T. Hays, *RF Superconductivity for Accelerators* (Wiley, New York, 1998).

[3] T. W. Haas, Surf. Sci. **5**, 345 (1966).

[4] T. W. Haas, A. G. Jackson, and M. P. Hooker, J. Chem. Phys. **46**, 3025 (1967).

[5] H. H. Farrell and M. Strongin, Surf. Sci. **38**, 18 (1973).

[6] H. H. Farrell, H. S. Isaacs, and M. Strongin, Surf. Sci. **38**, 31 (1973).

[7] B. M. Zykov, D. S. Ikonnoikov, and V. K. Tskhakaya, Sov. Phys. Solid State **17**, 2322 (1976).

[8] R. Pantel, M. Bujor, and J. Bardolle, Surf. Sci. **62**, 589 (1977).

[9] R. Fontaine, R. Caillat, L. Feve, and M. J. Guittet, J. Electron Spectrosc. Relat. Phenom. **10**, 349 (1977); J. M. Sanz and S. Hofmann, J. Less-Common Met. **92**, 317 (1983); F. A. Darlinsk and J. Halbritter, Surf. Interface Anal. **10**, 223 (1987).

[10] P. H. Dawson and Tam Wing-Cheung, Surf. Sci. **81**, 464 (1979).

[11] K. H. Rieder, Surf. Sci. **4**, 183 (1980).

[12] W. Yinsheng, W. Xuming, T. Zhijian, C. Yming, Z. Runsheng, T. Ushikubo, K. Sato, and Z. Shuxian, Surf. Sci. **372**, L285 (1997).

[13] M. Grundner and J. Halbritter, Surf. Sci. **136**, 144 (1984).

[14] J. Halbritter, Appl. Phys. A: Solids Surf. **43**, 1 (1987).

[15] A. Darlinski and J. Halbritter, J. Vac. Sci. Technol. A **5**(4), 1235 (1987).

[16] R. Franchy, T. U. Bartke, and P. Gassmann, Surf. Sci. **366**, 60 (1996).

[17] A. Daccà, G. Gemme, L. Mattera, and R. Parodi, Appl. Surf. Sci. **126**, 219 (1998).

[18] C. P. Flynn, W. Swieçh, R. S. Appleton, and M. Ondrejcek, Phys. Rev. B **62**, 2096 (2000).

[19] Ch. Sürgers and H. von Löhneysen, Appl. Phys. A: Solids Surf. **54**, 350 (1992).

[20] Ch. Sürgers, M. Schöck, and H. von Löhneysen, Surf. Sci. **471**, 209 (2001).

[21] H. Safa, D. Moffat, B. Bonin, and F. Koechlin, J. Alloys Compd. **232**, 281 (1996).

[22] B. R. King, H. C. Patel, D. A. Gulino, and B. J. Tatarchuck, Thin Solid Films **192**, 351 (1990).

[23] J. L. Womack, Chem. Modif. Surf. **3**, 269 (1990).

[24] F. Strisland, A. Ramstad, C. Berg, and S. Raaen, Philos. Mag. Lett. **78**, 271 (1998).

[25] I. Arfaoui, J. Cousty, and C. Guillot (to be published).

[26] I. Arfaoui, C. Guillot, J. Cousty, and C. Antoine (to be published).

[27] C. R. Brundle, Surf. Sci. **48**, 99 (1975); R. E. Ballard, J. Electron Spectrosc. Relat. Phenom. **25**, 75 (1982).

[28] M. Henzler, in *Electron Spectroscopy for Surface Analysis: Topics in Current Physics*, edited by H. Ibach (Springer-Verlag, New York, 1977), Vol. 4.

[29] J. H. van der Merwe, Surf. Sci. **449**, 151 (2000), and references cited.

[30] C. P. Flynn and J. A. Eades, Thin Solid Films **389**, 116 (2001).
[31] O. Hellwig, K. Theis-Bröhl, G. Wilhelmi, A. Stierle, and H. Zabel Surf. Sci. **398**, 379 (1998).
[32] O. Robach, I. K. Robinson, C. Durfee, B. W. Wiemeyer, and C. P. Flynn, Surf. Sci. **492**, 41 (2001).
[33] M. Batzill, D. E. Beck, and B. E. Koel, Appl. Phys. Lett. **78**, 2766 (2001).
[34] Y. Uehara, T. Fujita, M. Iwami, and S. Ushioda, Surf. Sci. **472**, 59 (2001).